

# Materials for semiconductor devices that can bend, fold, twist, and stretch

John A. Rogers

*This article is based on a presentation given by John A. Rogers for the Mid-Career Researcher Award on April 3, 2013, at the Materials Research Society Spring Meeting in San Francisco. Rogers received this award "for fundamental and applied contributions to materials, mechanics designs, and assembly techniques for stretchable/flexible electronic systems."*

New methods for the synthesis and deterministic assembly of advanced classes of nanomaterials enable integration of high-performence semiconductors with elastomeric substrates. These capabilities provide the foundations for a high-performance electronic and optoelectronic technology that can offer linear elastic mechanical responses to large strain deformations. The results create new opportunities in materials and device engineering, with important consequences in fields ranging from biomedicine to machine vision. This article summarizes the key materials science concepts and presents illustrative examples of their recent use in injectable, cellular-scale optoelectronic devices and in hemispherical compound eye cameras.

## Introduction

Research discoveries over the last 10 years provide routes to advanced electronic and optoelectronic systems that offer linear elastic mechanical responses to large-strain deformations.[1,2] Such devices can be bent, twisted, folded, stretched, and conformally wrapped onto arbitrarily curved surfaces without significant changes in operating characteristics. These properties lead to powerful, new engineering options and modes of integration, ranging from intimate mounting on tissues of the human body for surgical instruments, diagnostic monitors and human-machine interfaces, to configuration in complex, curvilinear, three-dimensional shapes for biologically inspired device designs. As a consequence, these technologies establish foundations for application possibilities that cannot be realized with devices built and packaged in the conventional way, on rigid printed circuit boards. The key challenge in materials science is to identify and optimize systems that can simultaneously provide high-performance semiconductor functionality and soft, compliant mechanics.

In addressing this goal, the primary difficulty is that the most well-developed electronic and optoelectronic materials, such as silicon and gallium nitride, are hard (moduli >100 GPa), brittle (fracture strains <1%), and only commercially available in the form of semiconductor wafers or planar thin films on wafer substrates. Two of the most successful strategies to address this problem exploit concepts of advanced composites, in a generalized sense of the term. The first uses dispersions of conducting or semiconducting nanoscale materials (i.e., nanowires, nanotubes, graphene, and others, or combinations of these) in elastomeric matrices. Here, two- or three-dimensional (2D/3D) networks form spontaneously in a way that can enable charge transport via flow through individual material elements and electrical junctions between them, with some level of control over important parameters such as the overall loading fraction and degree of alignment. The second exploits composites created deterministically by using ultrathin electronic materials lithographically defined into 2D ribbons, wires, or membranes. These structures are often induced into some modest level of 3D geometry by mechanical buckling and/or stacking. This approach offers the ability to integrate multiple materials into configurations with well-defined spatial layouts and engineered electrical contacts, both internal and external to the system.

An essential aim in the design of these classes of random and deterministic composites for stretchable electronics is to enable high loading fractions of a hard component, for high performance device functionality, with overall mechanics that remain dominated by a soft matrix for stretchable response. This goal is quite distinct from that associated with traditional composite engineering, where a hard material often serves to mechanically reinforce a surrounding matrix, and therefore demands attention to different types of considerations. A recent

John A. Rogers, University of Illinois, USA; jrogers@illinois.edu
DOI: 10.1557/mrs.2014.102

© 2014 Materials Research Society

https://doi.org/10.1557/mrs.2014.102 Published online by Cambridge University Press

issue of *MRS Bulletin* on stretchable electronics summarizes some of the most prominent approaches.[1] The following sections focus on results from my group, beginning with the essential ideas in materials science and concluding with recent examples of their use in materials engineering for biointegrated and bioinspired devices.

## Semiconductor nanostructures

Conventional inorganic semiconductor materials have large moduli and undergo brittle fracture at strains of ~1% or less. In the form of nanowires (NWs), nanoribbons (NRs), or nanomembranes (NMs), these same materials have bending stiffnesses and bending-induced strains (for a given radius of curvature) that are exceptionally small due to the cubic and linear scaling, respectively, of these quantities with thickness. Furthermore, the energy release rates associated with delamination between such nanomaterials and their supporting substrates are also small due to a linear dependence on thickness. These relationships (**Figure 1**a)[3] enable NWs/NRs/NMs to flex, conform, and bond robustly to nearly any surface and to be stacked onto one another or onto foreign hosts (e.g., plastic or rubber substrates) to yield unusual, heterogeneous systems that could not be achieved with wafer-bonding technologies or epitaxial materials growth. Although small thicknesses lead naturally to mechanical flexibility (Figure 1b), stretchability demands a linear elastic response to large strain deformation and therefore requires more sophisticated material configurations.

An effective route to stretchability with NWs/NRs/NMs exploits the mechanics associated with thin geometries (Figure 1a–b) to structure the materials into well-defined noncoplanar layouts and to bond them to elastomeric substrates.[4,5] Figure 1b shows an SEM image of an array of silicon NRs like those in Figure 1a, in "wavy" shapes created by a controlled process of buckling on a slab of poly(dimethylsiloxane) (PDMS).[5] Here, bonding between the silicon and PDMS occurs selectively in a pattern created by passing deep ultraviolet (UV) light through an unusual type of amplitude photomask that converts the unmodified hydrophobic surface of the PDMS, which is naturally dominated by $-CH_3$ and –H terminal groups, to a highly polar and reactive surface (i.e., activated surface), terminated with –OH and –O–Si–O– functionalities. This chemistry allows covalent interfacial reactions with various inorganic materials, including the native oxide surfaces of silicon NWs/NRs/NMs, to yield strong mechanical bonds upon physical contact, without the use of separate adhesives. The unexposed areas retain the unmodified surface chemistry (i.e., inactivated surface) and offer only weak van der Waals interactions with other materials. Relaxing the pre-strain induces compressive stresses in the

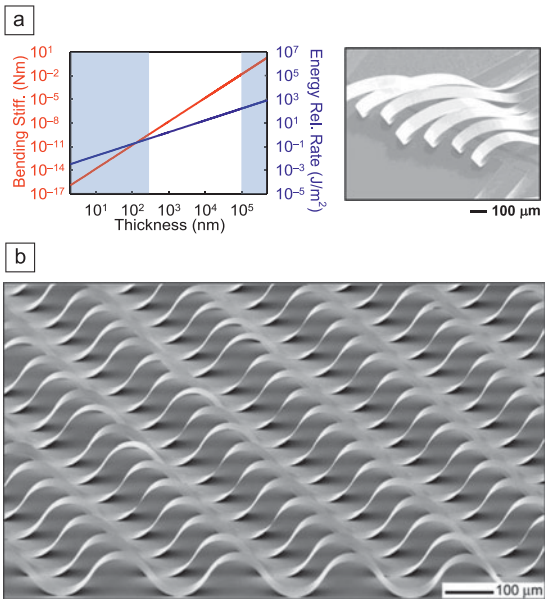



**Figure 1.** (a) The bending stiffness of a plate depends on the cube of its thickness. The red line corresponds to calculations for sheets of silicon with thicknesses between 2 nm and 200 μm. The shaded areas highlight regimes referred to as bulk wafers (right) and nanomembranes (NMs, left). The energy release rates associated with the opening of interfaces between such materials and their supporting substrates decrease linearly with thickness. The blue line represents calculations for Si NMs bonded to polyimide at room temperature, and then raised to 300°C. Reproduced with permission from Reference 3. © 2011 Nature Publishing Group. The frame on the right shows an SEM image of an array of flexible silicon nanoribbons (NRs) released by lateral etching near the surface of a wafer substrate. (b) SEM image of an array of silicon NRs in wavy configurations, formed by a controlled buckling process associated with release of prestrain in an underlying elastomer substrate. Lithographically defined surface chemistry on the elastomer leads to strong bonding to the NRs only at the positions of contact (i.e., the troughs of the wave structures). This composite material offers linear elastic response to applied strain, with overall mechanical properties defined by the elastomer. Reproduced with permission from Reference 5. © 2006 Nature Publishing Group.

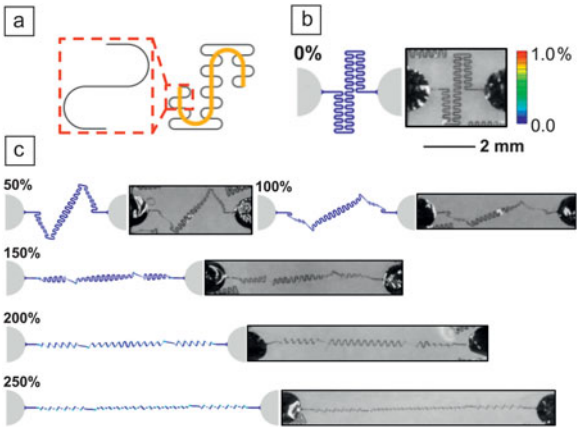



**Figure 2.** (a) Illustration of a representative "self-similar" serpentine structure (black: first level; yellow: second level). (b) Optical micrograph of such a structure (right) and layout for finite element modeling (left). (c) Optical images and corresponding finite element analysis of deformation at various levels of applied tensile strain. The color in the modeling results represents the maximum principal strains in the metal layer. Reproduced with permission from Reference 6. © 2013 Nature Publishing Group.


https://doi.org/10.1557/mrs.2014.102 Published online by Cambridge University Press

NRs to cause them to delaminate from the PDMS in the inactivated regions. The buckled, wavy layouts that result allow an effective, end-to-end stretchability in the resulting hard/soft composite structure, with a linear elastic mechanical response dominated by the PDMS. The wave structures reversibly change in amplitude and wavelength to accommodate either compression or tension, up to several tens of percent for this particular design, without fracture in the silicon. The physics is qualitatively much like that of an accordion bellows, where the elastomer provides a restoring force. For practical applications, a top layer of elastomer can be added to protect and encapsulate the silicon.

Advanced versions of these basic ideas can enhance the described behaviors. A recent example involves replacing the straight NRs of Figure 1 with filamentary serpentine traces in geometries referred to as "self-similar."[6] Here, buckling induces not only simple motions in the vertical direction, but also twisting deformations and sequential unfolding processes that significantly improve the levels of stretchability. Self-similar designs follow from iterative application of a single unit cell, in this case, a connected pair of horseshoe shapes (**Figure 2**a, red box), in orientations and scaled versions to reproduce the original geometry. The yellow line in Figure 2a highlights the long period component of a structure created by a single iteration of this process. Figure 2b illustrates an electrical interconnect with this type of design for use in a type of stretchable lithium-ion battery that might find applications in wearable electronics.[6] The points of bonding occur at the hemispherical disks to the left and right sides of the images. In this example, the serpentine consists of layers of polyimide (1.2 μm thickness) above and below a thin film of copper (0.6 μm). This stack places the metal at the neutral plane, thereby minimizing strains induced by bending during deformations that occur under stretching, as shown in Figure 2c.

Three-dimensional finite element analysis and experimental measurements illustrate the essential mechanics of this process for various levels of overall tensile strain. The self-similar geometry leads to a hierarchical, reversible buckling/unbuckling sequence that ensures low strains in the materials and elastic response, even under extreme stretching. For the range of cases shown in Figure 2c, configurations predicted by modeling agree remarkably well with those observed in the optical images. The physics involves a mechanism of "ordered unraveling,"[6,7] beginning with motion of the low frequency spatial Fourier component (second level) of the structure at a critical buckling strain of ~0.08%. This level gradually "unravels" via bending and twisting as the strain increases to ~150%, during which the high frequency component (first level) undergoes little deformation. The motions of the first level begin when the second level is almost fully extended, roughly at a strain of ~150%. Further increases in strain cause the first level to unravel, ultimately to a point that defines the limit in stretchability, corresponding to ~0.3% and ~1% strain in the copper for the onset of plastic deformation and fracture, respectively. Although many buckling modes exist, only the lowest order symmetric (Figure 2c) and anti-symmetric distributions of displacements appear in experiment. Modeling indicates that higher order modes have critical buckling strains that are more than twice as large as those associated with the lowest order modes.

Schemes for creating inorganic semiconductors in thin formats that allow access to the physics illustrated in Figures 1 and 2 range from mechanical exfoliation, for materials that

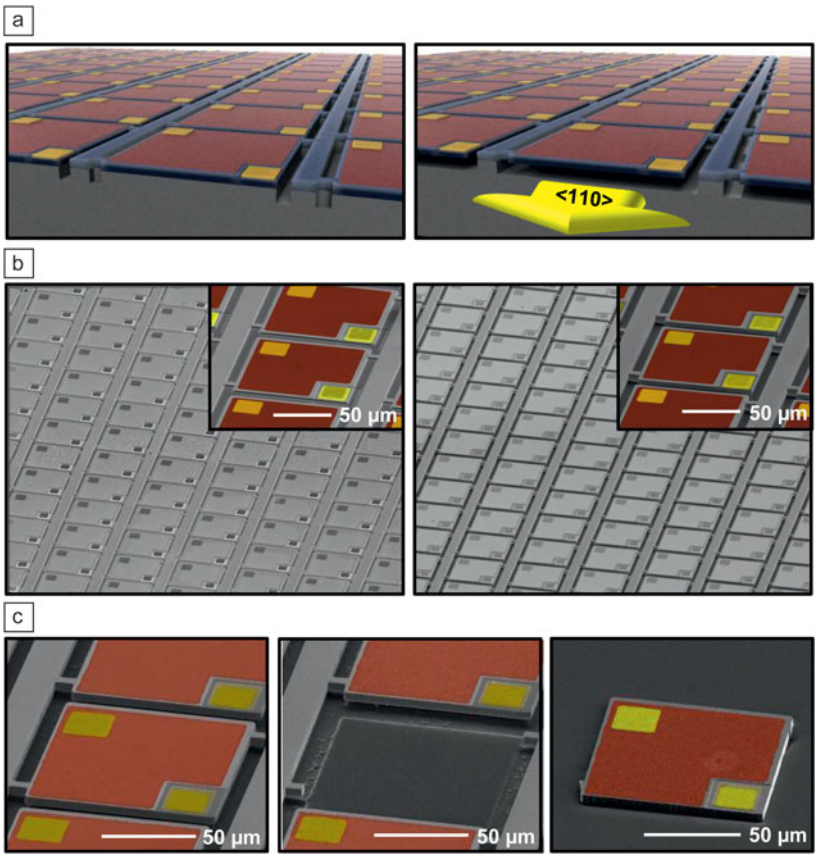



**Figure 3.** (a) Schematic illustration of an array of GaN μ-ILEDs before (left) and after (right) anisotropic etching of the near surface region of a supporting silicon (111) substrate. The colors correspond to InGaN (light blue), the contact pads (gold), and a thin current spreading layer (red). (b) SEM images of an array of GaN μ-ILEDs on a silicon (111) substrate before (left) and after (right) etching. The insets provide magnified views, colorized using a scheme similar to that in (a). (c) Colorized SEM images of a representative μ-ILED, shown after undercut (left), after removal from the silicon wafer (middle), and after delivery onto a receiving substrate (right). Reproduced with permission from Reference 10. © 2011 National Academy of Sciences.



https://doi.org/10.1557/mrs.2014.102 Published online by Cambridge University Press

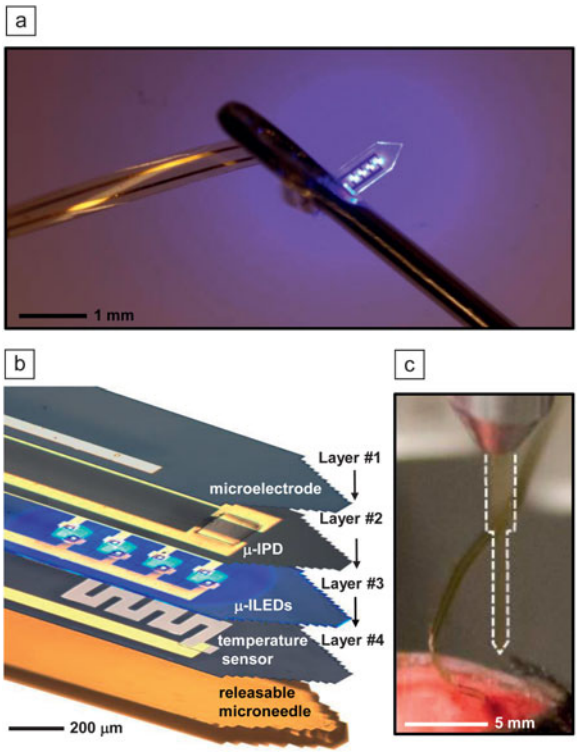



**Figure 4.** (a) Array of GaN μ-ILEDs on a thin, flexible filamentary polyimide substrate, threaded through and wrapped around the eye of a sewing needle. (b) A multifunctional, injectable optoelectronic device, shown as a series of tilted optical images, separated for ease of viewing. The system includes layers for electrophysiological measurement/stimulation (#1: Pt contact pad, microelectrode), optical measurement (#2: silicon μ-IPD), optical stimulation (#3: μ-ILED array), and temperature measurement and/or thermal stimulation (#4: serpentine Pt resistor), all bonded with a bioresorbable adhesive to a structural support for injection (releasable microneedle). (c) Picture of the final stage of injection into the depth of the brain, immediately after removal of the microneedle (perimeter of the microneedle is indicated with a dashed white line). Reproduced with permission from Reference 13. ©2013, AAAS.

naturally exist in layered forms, to chemical etching, for films that can be formed on sacrificial layers.[3] Other methods exploit anisotropy in the reactivity of bulk, single crystalline materials. For example, defining trenches on the surfaces of Si wafers with (111) orientations and then patterning their sidewalls with etch resists serves as a starting point for anisotropic removal of material along the ⟨110⟩ directions using solutions of potassium hydroxide (KOH), as either single layers or thick multilayer stacks.[8,9] Cycles of thermal oxidation and etching can reduce the thicknesses and passivate the interfaces of the NWs/NRs/NMs that result from this process. This scheme yields high-quality, device-grade semiconductor materials with smooth surfaces and thicknesses down to several nanometers.

## Functional microdevices

**Figure 3** illustrates a process that combines several of these ideas for releasing thin semiconductor structures, not just as material elements but as fully functional, ultrathin microdevices.[10] The method begins with GaN epitaxial layers grown on Si wafers with (111) orientation and then processed to form individual light-emitting diodes (LEDs), separated by narrow trenches that extend to a controlled depth (~1 μm) into the underlying silicon. The left frames of Figure 3a–b present schematic illustrations and SEM images, respectively, of a representative array. The procedures for release from the underlying substrate exploit anisotropic etching of the silicon, as described previously. In particular, when two sides of each LED are oriented perpendicular to the ⟨110⟩ direction, immersion in KOH rapidly undercuts the GaN without etching into the depth of the silicon. Because the etching proceeds only along ⟨110⟩, relief structures of silicon remain in the orthogonal (⟨111⟩) direction between the devices. A pair of small supporting structures of GaN connect each device to the underlying silicon to yield fully suspended configurations after the etching automatically terminates on the (111) planes. An illustration and corresponding SEM image appear in the right frames of Figure 3a–b, respectively. In these forms, the LEDs can be removed in a non-destructive, high-speed, and parallel operation using soft stamps and the techniques of transfer printing.[11] Deterministic assembly into arrayed layouts on nearly any substrate of interest can thus be achieved at room temperature, with throughputs of millions of components per hour and micron-scale positioning accuracy over areas that can be much larger than those defined by the wafer. The SEM

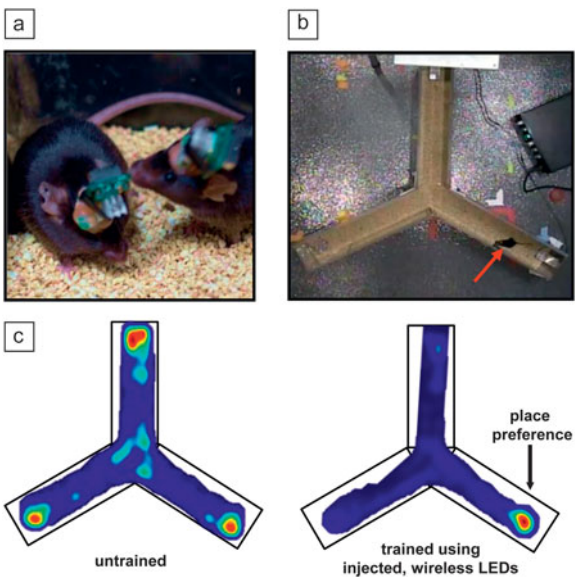



**Figure 5.** (a) Healthy, freely moving mice with lightweight wireless power supplies connected to arrays of GaN μ-ILEDs implanted near the ventral tegmental area of the brain (a group of neurons near the midline of the base of the midbrain). (b) Picture of a mouse (red arrow) with an injected μ-ILED system in a simple Y-maze environment. (c) Heat maps of activity in an untrained mouse (left) and a mouse optogenetically conditioned to exhibit a place preference for the right branch of the Y-maze (right). Reproduced with permission from Reference 13. © 2013 AAAS.


https://doi.org/10.1557/mrs.2014.102 Published online by Cambridge University Press

images in Figure 3c illustrate a progression from fabrication of the devices, to removal and printing onto a receiving substrate. The LEDs, which we refer to as microscale inorganic light-emitting diodes (μ-ILEDs), formed in this manner have emission areas (limited mainly by resolution in lithography) and thicknesses (a few micrometers) that can be many orders of magnitude smaller than those of conventional devices.

## Biointegrated optoelectronics for the brain

These and related ideas in materials, mechanics, and manufacturing science provide unique options for establishing intimate interfaces between advanced semiconductor devices and biology. Examples include systems formed on thin, soft elastomeric sheets with capabilities for non-invasive integration with the textured, dynamic surfaces of essential organs of the body, such as the skin, heart, and brain.[12] Similar strategies also allow for controlled introduction of microdevices into the depths of these and other tissues.[13] Here, thin, flexible components with dimensions at the scale of individual cells, or organelles, offer the ability to emit and detect light, measure temperature and introduce controlled heating, electrically stimulate and record, and perform other relevant operations. Transfer printing active materials onto thin, polymeric filaments yields mechanically compliant, multifunctional optoelectronic systems capable of injection into soft tissues. **Figure 4**a shows an image of a representative device of this type (GaN μ-ILEDs, ~6.45 μm thick, and 50 × 50 μm$^2$) threaded through and wrapped around the eye of a sewing needle for purposes of illustration. Miniaturized wireless powering modules and control schemes enable remote, untethered operation. These technologies significantly expand opportunities for use of optoelectronics technologies in biomedical engineering.

A recent example is in optogenetics, an emerging technique in neuroscience that allows cell-type selective control of neural pathways. The currently used fiber optic delivery structures constrain natural motions and prevent important types of behavioral studies on awake, ambulatory animal models. Figure 4b shows the layout of an injectable, wireless device structure designed for this application.[13] The system combines arrays of GaN μ-ILEDs created using the techniques of Figure 3, with co-located, precision optical detectors (microscale inorganic photodiodes, μ-IPD; silicon, 1.25 μm thick, 200 × 200 μm$^2$), thermal and electrophysiological sensors, and actuators. A releasable base, referred to as an injection microneedle, provides the necessary rigidity and physical toughness for penetration into the brain. A thin layer of purified silk fibroin, a protein derived from silkworm cocoons, serves as a bioresorbable adhesive that binds the multilayered device structure to this needle. Application of artificial cerebrospinal fluid immediately after injection dissolves the silk to allow removal of the microneedle, as shown in the right frame of Figure 4c. The exposed end of the polymer filament supports electrical contacts to an externally mounted, miniaturized wireless powering module. Such systems can deliver optoelectronic function directly to controlled locations in the depths of the brain without lasers, optics, fiber coupling systems, or optomechanical fixturing hardware.

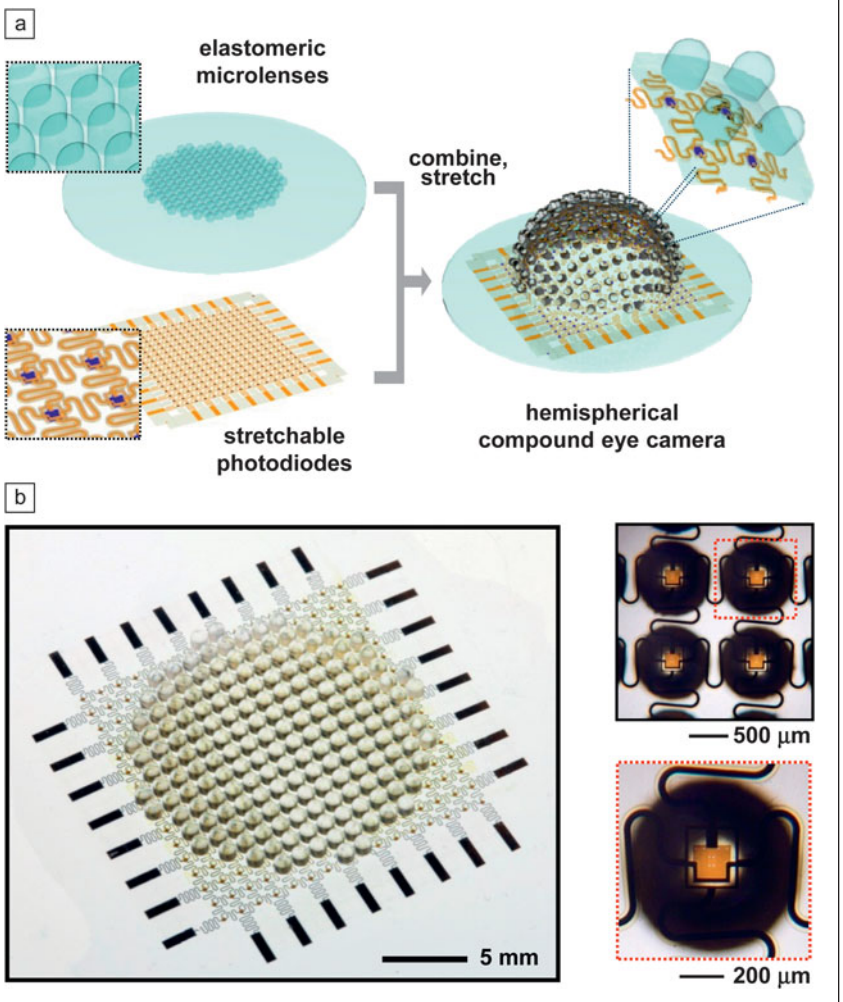



**Figure 6.** (a) Illustrations of an array of elastomeric microlenses and supporting posts joined by a base membrane (above; optical sub-system) and a corresponding array of silicon photodetectors interconnected by filamentary serpentine wires and configured for passive matrix readout (below; electrical sub-system). The left frame shows these sub-systems in their as-fabricated, planar geometries; the insets highlight four adjacent unit cells. Bonding these two sub-systems together and elastically deforming them into a hemispherical shape creates an apposition compound eye imager (center). An exploded view of four adjacent unit cells (i.e., artificial *ommatidia*) appears in the inset. (b) Picture of an integrated array, in planar format prepared for hemispherical deformation. The frames at the right provide an optical micrograph of four adjacent *ommatidia* (top) and a magnified view of one of them (bottom). Reproduced with permission from Reference 15. © 2013 Nature Publishing Group.



https://doi.org/10.1557/mrs.2014.102 Published online by Cambridge University Press

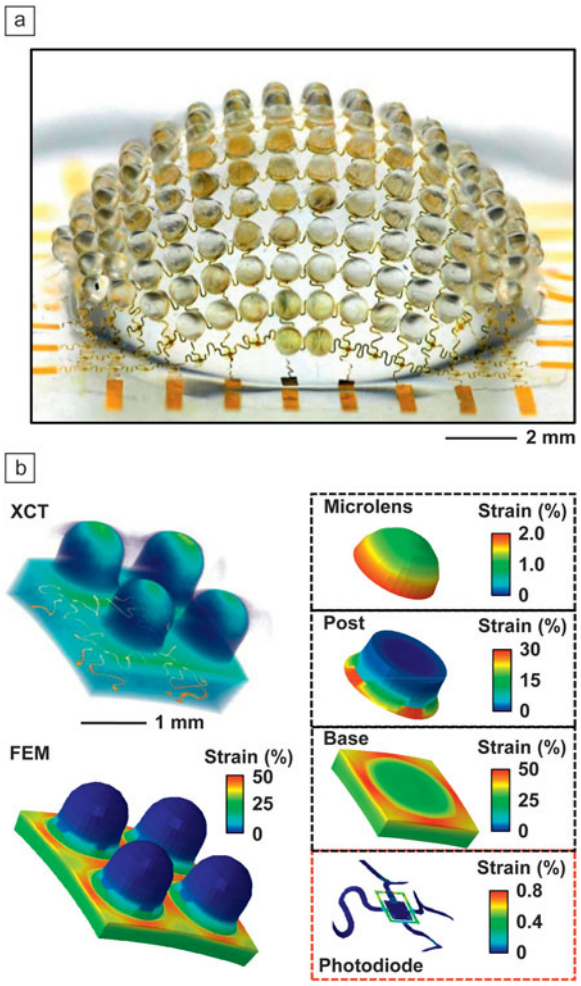



**Figure 7.** (a) Image of an integrated array of microlenses and interconnected photodetectors in a hemispherical configuration. (b) High resolution x-ray computed tomography (XCT) image of four adjacent *ommatidia* near the center of the camera (top left) and corresponding results from finite element modeling (FEM) (bottom left). The frames on the right illustrate computed strains in different components of an *ommatidium*: microlens (top), cylindrical supporting post (second from top), base membrane (second from bottom), and photodetector island with serpentine interconnects (bottom). Reproduced with permission from Reference 15. © 2013 Nature Publishing Group.

The cellular-scale dimensions of the components, the compliant mechanics, and the favorable thermal characteristics are all critically important for avoiding adverse biological responses in long-term use. The first two features minimize neuronal loss, reactive response of non-neuronal cells in the brain (glial cells) as well as tissue damage (gliosis) and immune reaction. A quantitative experimental study shows, in fact, substantially less glial activation and smaller lesion sites as compared to both metal cannulae and fiber optics, at both early (two weeks) and late (four weeks) phases.[13] The third feature is also critically important; it follows from the combined effects of (1) highly efficient heat spreading that results from the large surface area to volume ratios associated with thin, miniaturized devices, (2) active fluid cooling provided by natural blood flow in the vasculature of the surrounding tissue, and (3) robust optogenetic sensitivity at low duty cycle, pulsed mode operation with moderate peak powers. The maximum temperatures in regions directly adjacent to the μ-ILEDs, as measured *in vivo* with co-located, integrated temperature sensors (Figure 4b), are in the range of one-tenth of one degree, consistent with analytical modeling of the heat flow.[13,14] These temperatures are far lower than those known to cause adverse effects in brain tissue.

**Figure 5** shows implementation in animal models. The entire system, with wireless module, is compact and lightweight (~2.0 g), with no apparent constraint on natural behaviors.[13] Use of these devices in established optogenetics experiments, previously performed with fiber optic tethers, illustrates their effective operation. In one example, wireless control of μ-ILEDs in animals that express an appropriate channel rhodopsin (a class of protein that functions as light-activated ion channels) in the *locus coeruleus*, a brain region with known longitudinal noradrenergic cell bodies, leads to activation of dopaminergic neurons to yield salient stimuli sufficient for behavioral conditioning.[13] The result is an ability to train complex behaviors using only wirelessly triggered illumination from μ-ILEDs, without any physical reward. Figure 5b shows an example in which optogenetic conditioning of a mouse leads to a place-preference in a simple Y-maze. The time-integrated infrared image on the left frame of Figure 5c indicates that in the absence of training, the animals spend equal time in each of the three branches of the maze. Optogenetic stimulation can induce a place preference for the right branch, as shown in the right frame of Figure 5c, which persists even when the μ-ILEDs are not operating. Ongoing work exploits this technology in experiments that would be impossible with conventional optogenetic hardware, including those that involve complex, 3D environments and social interactions. More broadly, capabilities for biocompatible deep tissue injection of heterogeneously integrated optoelectronic systems have the potential to accelerate progress in many areas of basic research as well as in clinical treatment methods such as deep brain stimulation.

## Bioinspired digital cameras

Some of these concepts can also be exploited for bioinspired device design. One example is in digital cameras that adopt layouts found in the ocular organs (eyes) of arthropods, such as artificial compound eyes with full hemispherical coverage.[15] Here, the devices combine (1) an array of microlenses supported by cylindrical posts and joined by a base membrane, all of which are formed monolithically in a soft elastomer, and (2) a matching set of microscale silicon photodetectors in an open mesh layout with interconnects similar to those shown in Figure 2. Aligned bonding of these optical and electronic sub-systems together yields an integrated imaging array that exhibits a linear, elastic mechanical response to applied strains over a large range.


https://doi.org/10.1557/mrs.2014.102 Published online by Cambridge University Press

**Figure 6** shows the scheme and images of a representative device.[15] Alignment is accomplished using precision stages and microscopy systems adapted from those used in conventional mask aligners for photolithography. Controlled inflation allows geometrical transformation from the initial planar configuration, in which the devices are constructed, to a spherically curved shape with an adjustable radius of curvature, up to full hemispherical coverage for final use. Insertion of a rigid support to fix this shape and integration of a black matrix to prevent optical crosstalk between adjacent photodetectors completes the fabrication of a compound eye camera (**Figure 7**a).

This process of large-scale geometrical transformation must maintain precise optical alignment and avoid deform/fracture in the critical materials. Part of the solution to this challenge involves bonding the optical and electrical sub-systems only at the positions of the photodetectors using the type of selective surface chemistry described previously (Figure 1c). This scheme preserves the alignment and, at the same time, allows free motion of the serpentine interconnects in a way that minimizes their effects on the overall mechanics. The resulting response of the system to applied force is dominated by the elastic behavior of the PDMS used for the optical sub-system (modulus, ~1 MPa) and is nearly independent of the hard materials in the electronic sub-system (e.g., Si, ~150 GPa). Finite element modeling of the mechanics shows that the effective modulus of the system is only 1.9 MPa, and overall strains can reach more than 50% in equibiaxial tension before approaching the fracture thresholds of the electronic materials.[15]

The design of the optical sub-system itself is also important. Here, the modulus of the elastomer is sufficiently small, and the heights of the supporting posts are sufficiently large that deformations induced by stretching the base membrane are almost entirely mechanically decoupled from the microlenses. As a result, large strains created by geometry transformation induce no measurable change in the shapes or focusing properties of the microlenses. This isolating effect also minimizes strains at the locations of the photodetectors, thereby eliminating the possibility for fracture or delamination. These and other aspects of the mechanics[16] are highlighted in Figure 7 in an x-ray computed tomography image of a section of a device and in associated 3D finite element modeling of each component of the system.

In such cameras, light passes through each microlens/photodetector (i.e., artificial *ommatidium*) to yield a sampled image of the surroundings, with equal fidelity in all directions at once, and at a native resolution defined by the number of *ommatidia* (~180, for this example). A set of pictures, each collected at a slightly different orientation of the camera in both angular directions, enables composite renderings with improved effective resolution. This procedure simulates a process that is also likely adopted in biological systems.

The pictures obtained in this manner (**Figure 8**) exhibit only somewhat reduced edge resolution compared to results of rigorous optical simulations that assume ideal operation. Differences likely arise from parasitic scattered light in the cameras.[15] Quantitative demonstrations of the exceptionally large angular field of view that follows from the hemispherical layout can be performed through laser illumination across the camera, as shown in Figure 8b. The uniformity in size, brightness, and edge resolution of these spots is consistent with the expected behavior. These and other operational characteristics provide evidence of the high levels of sophistication that result from attention to all details of the materials, mechanics, and interfacial bonding chemistries. The outcomes yield fundamental insights into the operation of ocular systems in insects; they also suggest new options in camera design. The enabled fields of view, levels of aberrations, depths of focus, and high acuity to motion would be difficult or impossible to achieve using conventional approaches.

## Conclusion

New concepts in materials science like those illustrated here are rapidly opening up new possibilities in device engineering, with potentially important implications in areas of technology with broad societal value. Examples include biointegrated systems, such as "epidermal" sensors of physiological status, advanced surgical and diagnostic tools, implantable functional membranes and probes, and devices for wound healing

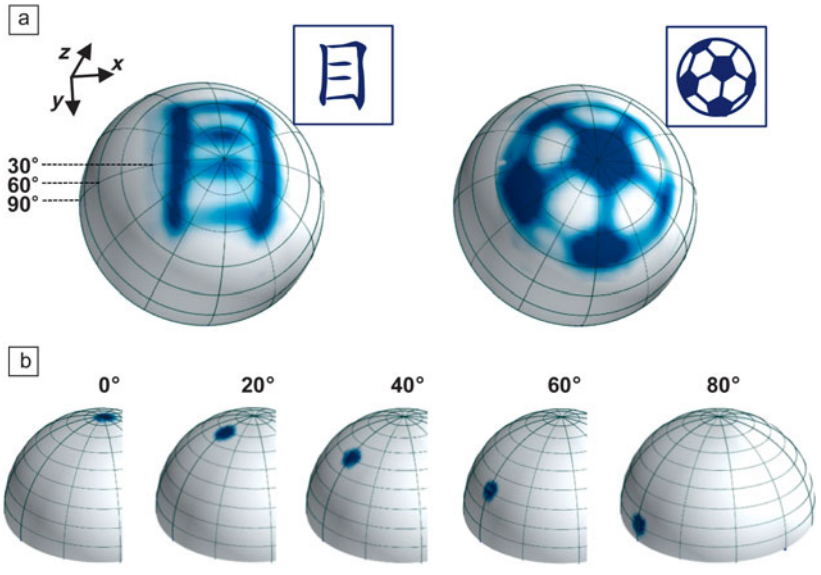



**Figure 8.** (a) Pictures of line art illustrations (insets) corresponding to the Chinese character for eye (left) and a soccer ball (right) captured with a hemispherical, apposition compound eye camera and rendered on a hemispherical surface. (b) Sequence of pictures corresponding to illumination of the camera with a collimated laser beam at different angles of incidence. Reproduced with permission from Reference 15. © 2013 Nature Publishing Group.



https://doi.org/10.1557/mrs.2014.102 Published online by Cambridge University Press

and burn management. Non-healthcare opportunities range from unusual lighting and photovoltaic systems, to structural integrity monitors (for bridges, airframes), to bioinspired imaging technologies and devices for adaptive camouflage. In all cases, fundamental developments in existing and new materials, including growth techniques, assembly methods, composite designs, processing strategies, structure/property relationships, integration schemes, and mechanical/electrical/optical properties will determine the rate of progress. The combined topics in both basic and applied science foreshadow a promising future for this emerging field of study.

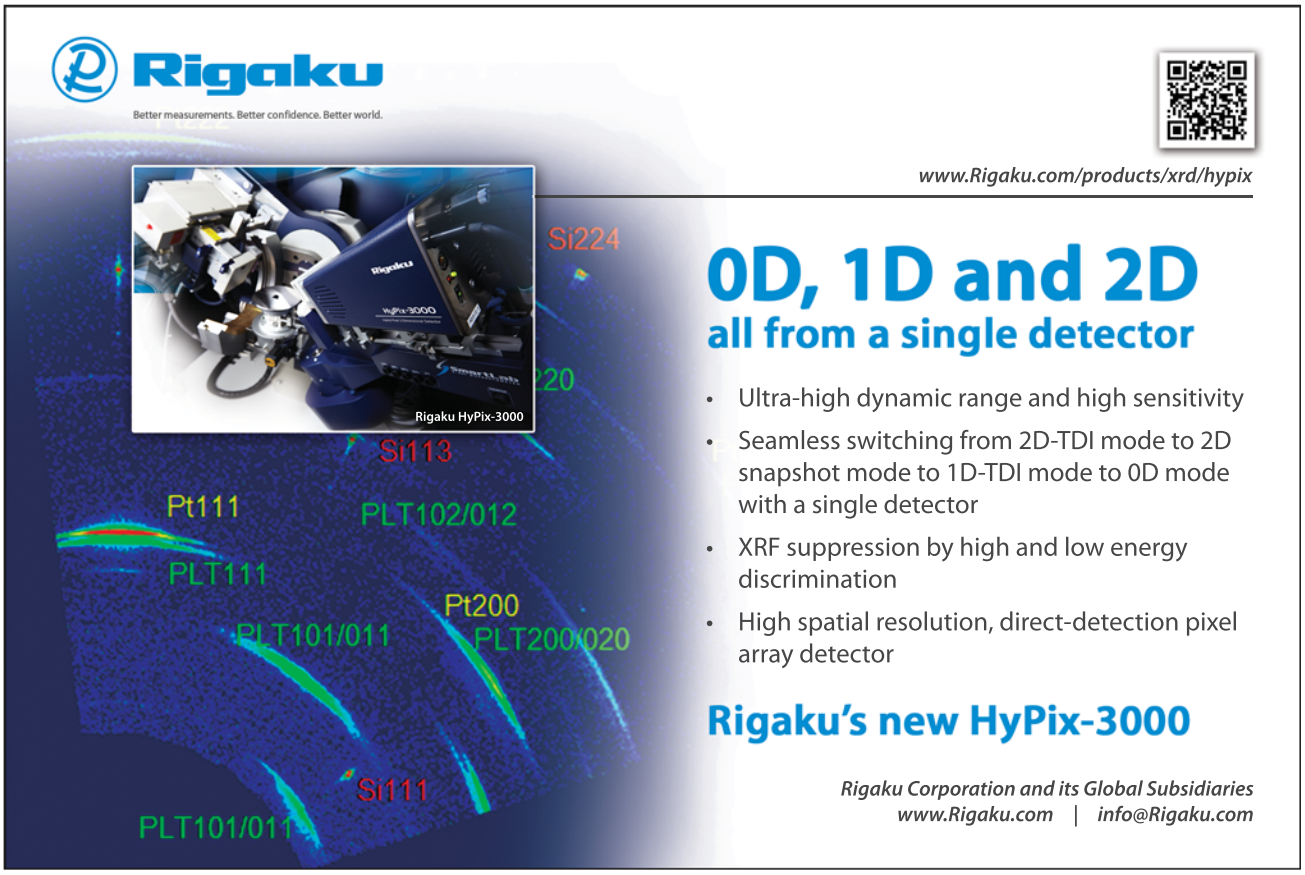
*To view a video of John A. Rogers' presentation at the MRS 2013 Spring Meeting, visit http://www.mrs.org/s13-mcr-video/.*

## References


1. S. Wagner, S. Bauer, *MRS Bull.* **37**, 207 (2012).
2. J.A. Rogers, T. Someya, Y. Huang, *Science* **327**, 1603 (2010).
3. J.A. Rogers, M.G. Lagally, R.G. Nuzzo, *Nature* **477**, 45 (2011).
4. D.Y. Khang, H. Jiang, Y. Huang, J.A. Rogers, *Science* **311**, 208 (2006).
5. Y. Sun, W.M. Choi, H. Jiang, Y. Huang, J.A. Rogers, *Nat. Nanotechnol.* **1**, 201 (2006).
6. S. Xu, Y. Zhang, J. Cho, J. Lee, X. Huang, L. Jia, J.A. Fan, Y. Su, J. Su, H. Zhang, H. Cheng, B. Lu, C. Yu, C. Chuang, T.-I. Kim, T. Song, K. Shigeta, S. Kang, C. Dagdeviren, I. Petrov, P.V. Braun, Y. Huang, U. Paik, J.A. Rogers, *Nat. Commun.* (2013); doi:10.1038/ncomms2553.
7. Y. Zhang, H. Fu, Y. Su, S. Xu, H. Cheng, J.A. Fan, K.-C. Hwang, J.A. Rogers, Y. Huang, *Acta Mater.* **61**, 7816 (2013).
8. S. Mack, M.A. Meitl, A.J. Baca, Z.-T. Zhu, J.A. Rogers, *Appl. Phys. Lett.* **88**, 213101 (2006).
9. H.C. Ko, A. Baca, J.A. Rogers, *Nano Lett.* **6**, 2318 (2006).
10. H. Kim, E. Brueckner, J. Song, Y. Li, S. Kim, C. Lu, J. Sulking, K. Choquette, Y. Huang, R.G. Nuzzo, J.A. Rogers, *Proc. Natl. Acad. Sci. U.S.A.* **108**, 10072 (2011).
11. A. Carlson, A.M. Bowen, Y. Huang, R.G. Nuzzo, J.A. Rogers, *Adv. Mater.* **24**, 5284 (2012).
12. D.-H. Kim, R. Ghaffari, N. Lu, J.A. Rogers, *Annu. Rev. Biomed. Eng.* **14**, 113 (2012).
13. T.-I. Kim, J.G. McCall, Y.H. Jung, X. Huang, E.R. Siuda, Y. Li, J. Song, Y.M. Song, H. An Pao, R.-H. Kim, C. Lu, S.D. Lee, I.-S. Song, G. Shin, R. Al-Hasani, S. Kim, M.P. Tan, Y. Huang, F.G. Omenetto, J.A. Rogers, M.R. Bruchas, *Science* **240**, 211 (2013).
14. Y. Li, X. Shi, J. Song, C. Lu, T. Kim, J.G. McCall, M.R. Bruchas, J.A. Rogers, Y. Huang, *Proc. R. Soc. London, Ser. A* **469**, 20130142 (2013).
15. Y.M. Song, Y. Xie, V. Malyarchuk, J. Xiao, I. Jung, K.-J. Choi, Z. Liu, H. Park, C. Lu, R.-H. Kim, R. Li, K.B. Crozier, Y. Huang, J.A. Rogers, *Nature* **497**, 95 (2013).
16. C.F. Lu, M. Li, J.L. Xiao, I. Jung, J. Wu, Y. Huang, K.-C. Hwang, J.A. Rogers, *ASME J. Appl. Mech.* **80**, 061022 (2013). □




**John A. Rogers** is the Swanlund Chair Professor at the University of Illinois, USA, and the Director of the Seitz Materials Research Laboratory. He received his PhD degree from the Massachusetts Institute of Technology and was a Junior Fellow in the Harvard University Society of Fellows. His is a Fellow of several professional societies, including MRS. He won a MacArthur Fellowship and the Lemelson-MIT Prize and is a member of the National Academy of Engineering and the American Academy of Arts and Sciences. Rogers can be reached by email at jrogers@illinois.edu.




https://doi.org/10.1557/mrs.2014.102 Published online by Cambridge University Press